Paper No.
04380

CORROSION2004

A PARAMETRIC STUDY AND MODELING ON LOCALIZED CO_2 CORROSION IN HORIZONTAL WET GAS FLOW

Yuhua Sun* **and Srdjan Nesic**
Corrosion in Multiphase Systems Center
Institute for Corrosion and Multiphase Technology
Ohio University, Athens, OH 45701, U.S.A

ABSTRACT

This study investigates localized CO_2 corrosion on carbon steels in wet gas services both experimentally and theoretically. A 100 mm I.D., 40 meter long flow loop is employed to perform the corrosion studies along the top and the bottom of the pipe under stratified and annular flow conditions. Various corrosion monitoring techniques, including ER, LPR, and WL, and surface analysis techniques, including SEM/EDS, MM, and XRD are used during the experiments and for post-test analysis.

The parametric study involves the systematic investigation for the effect of temperature, CO_2 partial pressure, Cl^-, pH, and flow regimes on localized corrosion and formation of corrosion product films. Localized corrosion is found only at high temperature (90°C) in both Cl^- containing and Cl^- free solutions (with different pitting density). It also occurs at lower pH (4.5~6.0) while at pH 6.2 very protective films form and no localized corrosion is identified. CO_2 partial pressure affects film formation and thus the localized corrosion when a partially protective film is formed. Corrosion behavior at the top approached that of the bottom when annular flow is maintained.

The theoretical study includes the development of a solution super saturation model and a scaling tendency model, which are good tools for predicting localized corrosion. Localized corrosion occurs when the solution is only slightly above the saturation point and when the scaling tendency is between 0.3 and 3.0.

Key words: localized CO_2 corrosion, carbon steel, wet gas, stratified flow, annular flow, super saturation, scaling tendency, iron carbonate film, surface analysis

---

* Current address: BP America Inc., Houston, TX 77079, U.S.A

INTRODUCTION

In the natural gas production industry, mild steel is extensively used for pipeline construction for economical reasons even though it has a relatively poor corrosion resistance. Natural gas does not emerge from the reservoir "pure" and is always accompanied by various amounts of oil, water, carbon dioxide, hydrogen sulfide or organic acids. These substances combined give rise to a very aggressive environment where the survival of mild steel is not guaranteed.

The multi-phase mixtures of gaseous and liquid hydrocarbons, water, CO_2 and H_2S moves through gas pipelines in a variety of complicated flow patterns such as annular, mist, slug and stratified flow, depending on the terrain topography and the individual phase flow rates. Flow can accelerate corrosion of mild steel by increasing the mass transfer of corrosive species and/or by damaging the protective films on the steel surface[1]. In wet-gas pipelines, the typical flow patterns mentioned above enhance the internal corrosion for both the top and the bottom of the pipe.

In the past 30 years, significant progress has been achieved in understanding uniform CO_2 corrosion of mild steel[2-7]. Localized corrosion is still not well understood even though most of the failures in lines are caused by localized attack, which is more difficult to predict or detect than uniform corrosion. In the field of wet gas corrosion research, there are only a handful of studies that relate to field experience, some focusing on corrosion management[8] and control [9], others reporting actual case histories[10]. In most studies the focus was on top-of-line corrosion[11,12] where high uniform corrosion and sometimes, localized attack, were associated with rapid condensation of water by external cooling. No studies investigated the nature and magnitude of the attack in wet gas transport in the presence of low condensation rates, typical for well-insulated pipelines.

Previous studies covering localized CO_2 corrosion of carbon steels have all been conducted in single-phase water flow[13-17]. A common underlying theme is that localized attack is always associated with the formation or breakdown of iron carbonate films. The apparatus used in those studies were the rotating cylinder electrode, jet impingement, autoclaves, and small diameter flow loops. They were not able to take into account the effect of multiphase flow and the presence of various flow regimes encountered in gas pipelines. Obviously, there is a gap between the single-phase flow laboratory corrosion studies and the multi-phase flow field application, which needs to be closed.

The present research was performed in an industrial-scale research facility - a 100 mm ID multiphase corrosion flow loop. The effect of various parameters on wet gas corrosion was systematically investigated, including temperature, pressure, solution composition, pH, and flow patterns. The most important parameters in the onset of localized attack of mild steel in wet gas transportation were also identified. A physico-chemical model was then developed based on the experimental findings. The results have improved the fundamental understanding and raised the awareness for localized corrosion in wet gas transportation.

EXPERIMENTAL

Flow Loop and Test Section

A unique, 18 m long, 100 mm diameter, high pressure, high temperature inclinable flow loop was employed to simulate gas production lines (Figure 1). The entire loop was manufactured from 316L stainless steel. A predetermined amount of liquid phase is stored in a 1.4 m^3 tank which serves as a storage tank as well as a separation unit for the multiphase gas/water mixture. The tank has a heating jacket and two 3 kW immersion heaters. Heat transfer oil is preheated in a separate tank by use of four

3.7 kW heaters and pumped through the heating jacket to heat the contents of the storage tank. Liquid is moved through this system by a stainless steel variable speed centrifugal pump. The flow is controlled within a range of 0 to 100 m^3/hr with the variable speed pump in conjunction with a recycling stream. Liquid is also pumped through a 25.4 mm I.D. bleed line to the progressive cavity gas pump (PCP) for "lubrication." This eventually flows back to the flow loop together with the gas. The flow rates in both the main line and the bypass line are metered with two inline turbine meters. Manual controlled valves are installed in each stream so that they can be adjusted when needed.

A gas feed line at 2 MPa pressure supplies carbon dioxide gas from a 20,000 kg storage tank. In normal operation, gas is continuously circulated through the system at desired speeds by a PCP, driven by a variable speed motor through a reduction gear system. A cooling jacket is installed in the gas line inlet to allow the temperature control during the normal operation. An exhaust line with a knock out drum is used to vent gas from the system if required.

The test section is a 100 mm diameter, 2 m long schedule 80 stainless steel pipe as shown in Figure 2. The three pairs of ports (A) at the top and at the bottom are used to insert flush-mountable electrical resistance (ER), linear polarization resistance (LPR), and weight loss (WL) probes for corrosion rate measurements. The pressure taps (C) are connected to pressure transducers and are used to measure the pressure drop for flow regime determination. The differential transducer taps are set up 7.0 m apart on the bottom of the pipe in this research. Ports for insertion of a pH probe (D), a sampling tube (C) and a thermocouple (B) are provided accordingly.

Specimen Preparation

All corrosion-monitoring probes were prepared the same way. In this research, ER probe was made from C1010, LPR probe was made from C1018, and two carbon steels, C1018 and X-65, circular with a diameter of 11.6 mm and a thickness of 3.1 mm, were used for WL and cross-sectional analysis. The chemical compositions of the steels are given in Table 1, Table 2, and Table 3.

Prior to testing, the specimen was polished by silicon carbide paper up to 600 grit, rinsed with isopropyl alcohol, and air drying. The specimen for weight loss analysis were weighed and numbered and then introduced into the system immediately.

The post-test cleaning procedure was performed by immediately rinsing the specimen with isopropyl alcohol, air drying, and then stored for surface analysis at a later time. For WL analysis, the specimen were pickled in an inhibited 10% hydrochloric acid for removal of corrosion products, then neutralized in alkali, rinsed with distilled water and alcohol, air dried and weighed for mass loss measurements. After this, the specimen was examined under a Metallurgical Microscope (MM) for the localized attack measurements.

For surface analysis specimens, after the surface of the specimen was examined by Scanning Electron Microscopy/Energy Dispersive Spectrum (SEM/EDS) and X-ray Diffraction (XRD), the specimens were prepared for cross-sectional analysis, to examine the thickness and morphology of the corrosion product film, and also provide another means to measure localized corrosion. This was achieved by first embedding the specimen into epoxy, followed by cutting across the specimen surface. A MM and/or SEM were used to generate photographs of the cross section.

Operational Procedure

The experimental system was filled with a predetermined amount of liquid solution and then heated to the test temperature. At the same time, the system was deoxygenated by flushing carbon

dioxide through the system until the level of dissolved oxygen was below 10 ppb. The system was then pressurized to the test pressure. The flow rates of the gas and liquid were set separately. The pH was then adjusted by adding either $NaHCO_3$ or HCl into the flow loop. Once the flow was stabilized, corrosion-monitoring probes were inserted into the test section under pressure. The tests lasted from a few hours for low temperature 40°C tests up to 200 hours for high temperature 90°C tests, aiming at establishing a stabilized general corrosion rate in the presence of surface films. The test matrix for this work is shown in Table 4.

EXPERIMENTAL RESULTS AND DISCUSSIONS

The monitoring and analysis of corrosion rate and other important process parameters (pH, Fe^{2+} etc.), as well as the comparisons and discussions among different measurement techniques (ER, LPR, and WL), have been presented elsewhere[18]. The parametric study of the current research will focus only on the final results.

The Effect of Temperature

Figure 3 shows the effect of temperature on corrosion rate from ER and WL methods for both the top and the bottom of the pipe. The flow was in stratified flow regime. It is seen that localized corrosion did not occur at a low temperature of 40°C on either the top or the bottom of the pipe. However, at a high temperature of 90°C localized corrosion on the bottom of the pipe occurred, and no localized corrosion on the top was observed. Thus the focus is shifted more to the high temperature tests in the following discussions.

It is observed that the corrosion rate for the bottom of the pipe varied greatly from 40°C to 90°C. The corrosion rate increases with the increase in temperature due to the higher reaction rate at higher temperature. In this particular test, a corrosion product film had formed at 90°C, as indicated in Figure 4. The specimen surface was covered by a crystalline layer, which was identified later as $FeCO_3$ (XRD results shown in Figure 5). However, the corrosion product film formed at this condition had some local defects and failures and thus was considered to be non-protective. The corrosion rate remained high at over 12 mm/yr, and localized corrosion was initiated at the sites of local film failure. At 40°C, no $FeCO_3$ film was formed, as shown in Figure 6.

The corrosion rate at the top of the pipe did not vary much with the change of the temperature. At the test conditions, the flow was in stratified flow regime. In this flow regime, some condensation occurs, even if the pipe was insulated, and liquid droplets entrained in the gas phase can impact the top of the pipe wall. At 40°C, the condensation on the top of the pipe was almost negligible[19], thus it is speculated that the corrosion rate was mainly contributed due to the liquid droplets impinging on the wall, as the condensed water is more corrosive. At 90°C, although the condensation rate was higher, the small amount of water on the top might have become soon saturated by the corrosion product due to the higher reaction rate and lower solubility of $FeCO_3$ at this temperature. Thus the corrosion rate shows a larger difference between the top and bottom at 90°C compared to 40°C under stratified flow conditions. The error bars shown in the plots were evaluated by experimental uncertainty analysis described elsewhere[20]. Generally, a higher corrosion rate, longer test time, higher sensitivity of the probes, and more stable test temperature lead to less variability and more accurate corrosion rate measurements.

The Effect of Cl^-

Figure 7 shows the effect of NaCl concentration on the bottom corrosion rate from WL method for both C1018 and X65 materials. It is seen that Cl^- had some effects on both uniform and localized

corrosion rate on the bottom of the line. In all cases, localized corrosion occurred on both materials. However, Figure 7 cannot tell more about the nature of the localized attack. In fact, some of the localized attack was widespread on the specimen surface, with hills, valleys, and mesa typed corrosion covering the whole surface (

Figure **8**), while on others it was a true local phenomenon (Figure 9). Based on this consideration, the concept of pitting density was proposed to describe the localized corrosion. The pitting density is defined as the ratio of pitted area to the total area of specimen. The results are shown in Figure 10. Higher Cl^- concentration seems to cause lower pitting density and the localized corrosion tends to be more "local". C1018 and X65 have different sensitivities with respect to the Cl^- concentration.

This series of tests were performed under stratified flow conditions. Neither C1018 nor X-65 suffered localized attack at the top of the line. The corrosion rate was orders of magnitude lower than the bottom, as shown in Figure 11. The water chemistry on the top of the line was different from the bottom under stratified flow conditions. The water on the top of the pipe could be from two sources: either from the droplets entrained in the gas phase, which should have the same chemistry as the water at the bottom; or from the pure condensing water, whose chemistry is very different. However, according to the cross-section images (Figure 9a and 9b), the amount of water on the top must have been very small, enabling formation of a very thin liquid film, which was rapidly saturated by $FeCO_3$ and lead to a protective layer. This layer was not affected by the presence of Cl^-. Admittedly the concentration of Cl^- at the top was most likely lower due to the presence of condensed water. Thus no localized corrosion was found on the top and the uniform corrosion rate remained low.

The Effect of CO_2 Partial Pressure

With film free conditions at 40°C, no localized corrosion was identified at any pressure investigated. The general corrosion rate increased with the increase in CO_2 partial pressure for both the top and the bottom, as shown in Figure 12. The corrosion rate on the bottom followed a 0.7 power in relation to CO_2 partial pressure, as previously suggested in the literature[3,21]. The corrosion rate on the top was small at low pressure up to 8 bars but dramatically increased with rising CO_2 partial pressure. The power law did not apply on the top corrosion rate mostly because of the flow regime changed with the change of pressure. At low pressure, the flow was in stratified with only occasional droplets hitting on the top of the pipe wall; at high pressure, the flow pattern changed from stratified to semi-annular or annular flow, the top of the pipe started to see the same water phase as the bottom, and the corrosion rate went up consequently.

With film forming conditions at 90°C, localized corrosion was identified at lower pH of less than pH 5.2, as shown in Figure 13 and

Figure **14**. Localized corrosion only occurs on the bottom under lower pressure 3.8 bar when stratified flow forms, but it occurs everywhere under higher pressure 10.6 bar when annular flow forms. Under the same flow velocities, high pressure led to the formation of annular flow, which had caused the same water chemistry for both the top and the bottom of the pipe. The corrosion product film formed in such conditions was not protective and localized corrosion was initiated. However, higher CO_2 partial pressure increases the rate of film formation and facilitate more protective film formation, as can be seen from Figure 15. The stabilized bottom corrosion rate was decreased by two orders of magnitude with the increase in CO_2 partial pressure. Nesic et al.[22] made similar conclusions based on the predictions from their mechanistic film growth model. However, as can be seen from above figures, localized corrosion occurred on the top of the line at high pressure, although the stabilized uniform corrosion rate was very low (0.06 mm/yr). The very low uniform corrosion rate does not guarantee safe operation due to possible localized attack. Thus the real corrosion risk cannot be determined simply from the uniform

corrosion rate. This becomes extremely important in field applications, where ER probes are very often used to monitor the corrosion rate. Once localized corrosion takes place, it is always much higher than the uniform corrosion rate measured by ER technique.

With film forming conditions at higher pH 6.2, no localized corrosion was identified, as can be seen from Figure 16 and Figure 17, the corrosion product film can be considered fully protective. Under controlled high pH environments, the increase in CO_2 partial pressure did not change the corrosion rate on the bottom, but it decreased the corrosion rate on the top. At high pressure, the flow was in annular flow regime, and the top of the line also had high pH. But in stratified flow, as in the low-pressure conditions, the top of the line suffered from condensation at the beginning and resulted in a higher average corrosion rate. However, once the fully protective film formed, the corrosion rate was unresponsive to the change of CO_2 partial pressure for both the top and the bottom, as can be seen in Figure 18. The stabilized corrosion rates were the same for different pressures, and they were all below 0.1 mm/yr.

The Effect of pH

A relatively low pH environment can apparently initiate the localized attack. Under stratified flow regime, localized corrosion occurred only on the bottom as shown in Figure 19. The water on the top must have a different chemistry due to the condensation. However, when the water was spread around the pipe wall as in annular flow, which caused the same pH everywhere in the pipe, localized corrosion took place on both the top and bottom, as indicated in Figure 20. Thus the issue of whether the top of the line would suffer localized attack largely depends on the flow regime and the local pH. Under a higher pH environment, localized corrosion was inhibited in both the top and the bottom in both flow regimes. The most important pH contribution is that it largely affects species concentration in solution. This might further affect the solution super saturation level and, finally, scaling tendency.

Uniform corrosion was also largely affected by the change of pH and flow regime. As can be seen from Figure 21 and Figure 22 with the stabilized corrosion rate (stable for more than 50 hours), the corrosion rates dropped dramatically with the increase of pH for both flow regimes. The corrosion rates on the top and the bottom were much closer to each other in annular flow, which is understandable due to the same water chemistry. The difference of corrosion rate from the top to the bottom might be attributed to the dissimilar water film velocities near the pipe wall.

Under stratified flow, the corrosion rate on the top was more than an order of magnitude lower than the bottom corrosion rate at low pH. On the contrary, at high pH, the corrosion rate on the top was more than a factor of two higher than the bottom corrosion rate. As addressed before, the top of line experienced a stronger influence of water condensation in stratified flow. The distinct water chemistry from the bottom to the top can explain the discrepancy in corrosion rate. However, the question arose: does the water on the top come entirely from condensation under stratified flow regime? If the answer was yes, then one should not see any difference with the change of pH in the solution, given that all the other test parameters remain the same, e.g., superficial velocities, temperature, pressure etc. The condensed water on the top should not be able to “sense” the pH change in the bulk water at the bottom. Nevertheless, in Figure 21, the corrosion rate actually decreased four times when the pH was increased. This suggested that a portion of the water on the top must be from the water droplets that have the same pH as the bottom water. Thus the issue “where the water is from” on the top of the line in stratified flow can now be resolved. The answer is: it is from both condensation and water droplets impingement.

In the oil and gas industry, a pH 4 to 6 is of primary practical interest since it represents the majority of environments in pipeline transportation. Since localized corrosion is of large concern, pH stabilization technique should be considered as a method to combat it.

PHYSICO-CHEMICAL MODEL DEVELOPMENT

After reviewing all the tests with the numerous influential factors, it was found that localized corrosion only occurs at certain conditions where corrosion product film formed but was incapable to provide sufficient protectiveness. The graphical illustration is as below:

no film	partially protective film	fully protective film
High uniform attack No localized attack	Low/high uniform attack Localized attack	Low uniform attack No localized attack

The two extreme conditions, white and black area, result in uniform corrosion. Localized corrosion may occur only in a so-called "gray zone" area, where the corrosion product film is formed but cannot offer satisfactory protection. For more practical reasons, knowing the risk of localized corrosion (i.e. borders of the gray zone) is probably more important than knowing the magnitude of the localized corrosion rate. Hence, the model development will focus on identifying the risk of occurrence of localized corrosion. Under fixed temperature and pressure conditions, localized corrosion seems to be closely related to the solution properties, such as the iron super saturation level and the scaling tendency.

Super Saturation (SS) Level and Localized Corrosion

The iron super saturation level (SS) is defined as follows:

$$SS = \frac{\left[Fe^{2+}\right]\left[CO_3^{2-}\right]}{K_{sp}} \tag{1}$$

where, $[Fe^{2+}]$ represents the equilibrium ferrous ion concentration in mol/l, which was experimentally measured in each test; $[CO_3^{2-}]$ represents the equilibrium concentration of carbonate ion in mol/l, which was computationally determined; K_{sp} is the solubility product of iron carbonate, which is the function of temperature and solution ionic strength expressed as[23]:

$$pK_{sp} = 10.13 + 0.0182 * T - 2.44 * I^{0.5} + 0.72 * I \tag{2}$$

where, T is the temperature in Celsius and I is the ionic strength in mol/l. The ionic strength is defined by G.N. Lewis[24] as:

$$I = \frac{1}{2}\sum_i m_i z_i^2 = \frac{1}{2}\left(m_1 z_1^2 + m_2 z_2^2 + \ldots\right) \tag{3}$$

where m is the species concentration in mol/l, and z is the species charge.

In most of the tests, the solution chemistry changed more or less from the beginning to the end of the test due to iron dissolution. Thus the super saturation level at both the beginning and the end of the test were calculated separately for each test. The relationship between the super saturation level and localized corrosion is plotted in Figure 23 and Figure 24.

Figure 23 shows one way to present the localized corrosion by use of the pitting factor. The pitting factor *f* is defined as follows:

$$f = \frac{CR_{\max} - CR_{aver}}{CR_{aver}} \quad (4)$$

A pitting factor of zero suggests no localized corrosion, while any number above zero indicated the occurrence of localized attack. It is interesting to observe that localized corrosion took place whenever the solution started under saturated and ended up mildly supersaturated. There are two groups of data points, indicated by small arrows in Figure 23, when both the beginning and the end of experimental points are either well below or well above the saturation point, there was no localized corrosion with a pitting factor of zero. These data represent the low temperature of 40°C tests and high temperature (90°C)/high pH (6.2) tests, respectively. The two cases represent the two extreme conditions: either no film was formed (40°C) or fully protective film was formed (90°C, pH 6.2). In addition, a solid line can be seen in Figure 23. This line envelopes a range within which localized corrosion is most likely to occur. It also shows that the pitting factor gets bigger when the super saturation is closer to 1, due to the poorest protection offered by precipitating film.

Figure 24 presents another way to describe the localized corrosion by pitting density. A pitting density of zero expresses no localized corrosion, while any value above zero indicates the occurrence of localized attack. It is seen that most of the localized attack has the pitting density less than 10% of the total area, which illustrates that the localized attack is genuinely a local phenomena. In addition, the solid line envelopes a range within which localized corrosion can occur. It also shows that the pitting density gets smaller when the super saturation level is closer to 1, which suggests that the localized corrosion tends to be more "local", and deeper (Figure 23).

Therefore, the super saturation level is a crucial factor for localized corrosion from two perspectives: magnitude and density. When the solution is close to the saturation point with respect to iron carbonate, the steel tends to be locally and highly attacked. Thus the super saturation model for localized corrosion can be summarized as:

If SS<1 or SS>>1	uniform corrosion
If 1<SS<3	localized corrosion possible

Scaling Tendency and Localized Corrosion

van Hunnik[25] and Pots[26] proposed a "scaling tendency" (ST) concept to describe the likelihood of protective film formation. It is defined as follows:

$$ST = \frac{PR}{CR} \quad (5)$$

where, PR is the iron carbonate precipitation rate and CR is the corrosion rate expressed in the same units. They also found when *ST >2* (with both PR and CR expressed in volumetric units), a protective film is considered to form. According to the experimental findings in this research, localized corrosion occurred when a non-protective film formed. Therefore, using the same concept, the corrosion rates (initial CR) experimentally measured in mm/yr was compared to the precipitation rate in mm/yr, which was calculated by the following equation[25,26]:

$$\left[Fe^{2+}\right]_{prec} = k_r K_{sp}\left(SS - 1\right)\left(1 - SS^{-1}\right) \quad \mathbf{(6)}$$

where, k_r is the temperature dependent rate constant.

The prerequisite for the film formation is a super saturated solution. Any under saturated solution will not lead to film formation and the scaling tendency should be zero. The relationship between the super saturation level and localized corrosion is plotted in Figure 25. The pitting factor seems large around scaling tendency of 1, which corresponds to poorly protective films. According to Figure 25, the scaling tendency model for localized corrosion can be summarized as:

If ST<<0.3 or ST>>3	uniform corrosion
If 0.3<ST<3	localized corrosion possible

CONCLUSIONS

Parametric study through the experiment results indicates that localized corrosion occurs only when partially protective films are formed. Under film free or formation of fully protective films, only uniform corrosion takes place.

Temperature affects the corrosion product film formation and thus localized corrosion. At low temperature of 40°C, no localized corrosion occurred and no iron carbonate corrosion product films were identified. At high temperature of 90°C, corrosion product films can vary significantly: fully protective films resulted in no localized corrosion while partially protective films caused localized attack.

The CO_2 partial pressure played various roles with respect to the formation of corrosion product films under various conditions. Under film free conditions, the uniform corrosion rate increased with the increase in CO_2 partial pressure. With the formation of fully protective films, the corrosion rate was unresponsive to the change of CO_2 partial pressure within a large range. With partially protective films, the increase in CO_2 partial pressure might have facilitated the formation of more protective films and resulted in less localized attack in both magnitude and pitting density.

Localized corrosion was observed under both Cl^- free and Cl^- containing solutions. The Cl^- concentration affected the localized corrosion through pitting density.

Solution pH was critical to localized corrosion. It was found that pH 6.2 or higher can inhibit the localized corrosion, while pH in the range 4.5<pH<6.0 may trigger localized attack.

X65 was somewhat more resistant to localized corrosion than C1018 in general. However, no systematic advantage of one over the other was observed.

A solution super saturation level and/or scaling tendency can both be used to describe the likelihood of localized corrosion. It is found that localized corrosion occurs when the solution is above the saturation point and less than 3. Under these conditions the scaling tendency is typically between 0.3 and 3.0. Indeed, calculating or measuring solution super saturation is much easier and entails a smaller error and therefore is recommended as means of predicting the risk of localized corrosion.

ACKNOWLEDGEMENTS

The authors would like to thank the member companies of the Institute for Corrosion and Multiphase Technology at Ohio University for the final support in this research.

REFERENCES

1. Nesic, S., Nordsveen, M., Nyborg, R., and Stangeland, A., "A Mechanistic Model for CO_2 Corrosion with Protective Iron Carbonate Films," Corrosion/2001, paper no.40, (Houston, TX: NACE International, 2001).
2. de Waard, C., and Milliams, D.E., " Carbonic Acid Corrosion of Steel," *Corrosion*, 31(5), p.197, 1975.

3. Dugstad, A, Lunde, L., and Videm, K., "Parametric Study of CO_2 Corrosion of Carbon Steel," Corrosion/94, paper no.14, (Houston, TX: NACE International, 1994).
4. Vuppu, A.K., and Jepson, W.P., " Study of Sweet Corrosion in Horizontal Multiphase Carbon Steel Pipelines," Offshore Technology Conference, 1993.
5. Bhongale, S., " Effect of Pressure, Temperature, and Froude Number on Corrosion Rates in Horizontal Multiphase Slug Flow," Master's thesis, Ohio University, 1995.
6. Nesic, S. and Lunde, L., " Carbon Dioxide Corrosion of Carbon Steel in Two-phase Flow," *Corrosion*, 50 (9), p.717, 1994.
7. Palacios, C.A and Shadley, J.R., " Characteristics of Corrosion Scales on Steels in a CO_2-saturated NaCl Brine," Corrosion, 47 (2), p.122, 1991.
8. Kapusta, S.D., Pots, B.F.M., and Connell, R.A., "Corrosion Management of Wet Gas Pipelines," Corrosion/99, paper no.45, (Houston, TX: NACE international, 1999).
9. Gunaltun, Y.M. and Belghazi, A., "Control of Top of Line Corrosion by Chemical Treatment," Corrosion/2001, paper no. 33, (Houston, TX: NACE International, 2001).
10. Gunaltun, Y.M., Supriyatman, D., Achmad, J., "Top of line corrosion in multiphase gas lines, A case history," Corrosion/99, paper no. 36, (Houston, TX: NACE International, 1999).
11. Gunaltun, Y. M., and Larrey D, "Correlation of cases of top of line corrosion with calculated water condensation rates," Corrosion/2000. paper no.71, (Houston, TX: NACE International, 2000).
12. Pots, B.F.M, and Hendriksen, E.L.J.A. "CO_2 Corrosion Under Scaling Conditions- The Special Case of Top-Of-Line Corrosion in Wet Gas Pipelines," Corrosion/2000, paper no.31, (Houston, TX: NACE International, 2000).
13. Xia, Z., Chou, K.C., and Szklarska-Smialowska, Z., "Pitting Corrosion of Carbon Steel in CO_2-Containing NaCl Brine," *Corrosion*, 45 (8), p.636, 1989.
14. Schmitt, G., Guddle, T., Strobel-Effertz, E., " Fracture Mechanical Properties of CO_2 Corrosion Product Scales and Their Relation to Localized Corrosion," Corrosion/96, paper no.9, (Houston, TX: NACE International, 1996).
15. Schmitt, G., Mueller, M., "Critical Wall Shear Stresses in CO_2 Corrosion of Carbon Steel," Corrosion/99, paper no.44, (Houston, TX: NACE International, 1999).
16. Schmitt, G., Bosch, C., and Mueller, M., " A Probabilistic Model for Flow Induced Localized Corrosion," Corrosion/2000, paper no. 49, (Houston, TX: NACE International, 2000).
17. Nyborg, R., "Initiation and Growth of Mesa Corrosion Attack During CO_2 Corrosion of Carbon Steel," Corrosion/98, paper no.48, (Houston, TX: NACE International, 1998).
18. Sun, Y., George, K., and Nesic, S., "The Effect of Cl^- and Acetic Acid on Localized CO_2 Corrosion in Wet Gas Flow," Corrosion/2003, paper no.328, (Houston, TX: NACE International, 2003).
19. Vitse, F., "Experimental and Theoretical Study of the Phenomena of Corrosion by Carbon Dioxide under Dewing Conditions at the Top of A Horizontal Pipeline in the Presence of Non-condensable Gas," Dissertation, Ohio University, 2002.
20. Sun, Y., "Localized CO_2 Corrosion in Horizontal Wet Gas Flow," Dissertation, Ohio University, 2003.
21. de Waard, C., and Lotz, U., "Prediction of CO_2 Corrosion of Carbon Steel," Corrosion/93, paper no.69, ((Houston, TX: NACE International, 2003).
22. Nesic, S., Lee, K-L. J., and Ruzic, V., "A Mechanistic Model of Iron Carbonate Film Growth And The Effect on CO_2 Corrosion of Mild Steel," Corrosion/2002, paper no.02237, (Houston, TX: NACE International, 2002).
23. http://www.nts.no/norsok.
24. Daniels, F., and Alberty, R.A., *Physical Chemistry*, 3rd edition, John Wiley & Sons Inc., New York, 1996.

25. van Hunnkik, E.W.J., Pots, B.F.M., and Hendriksen, E.L.J.A, "The Formation of Protective $FeCO_3$ Corrosion Product Layers in CO_2 Corrosion," Corrosion/96, paper no.6, (Houston, TX: NACE International, 1996).
26. Pots. B.F.M., and Hendriksen, E.L.J.A., "CO_2 Corrosion Scaling Conditions-The Special Case of Top-Of-Line Corrosion in Wet Gas Pipelines," Corrosion/2000, paper no.31, (Houston, TX: NACE International, 2000).

TABLE 1 CHEMICAL COMPOSITION OF C1010 CARBON STEEL (WT.%) (FE IS IN BALANCE).

Al	As	B	C	Ca	Co	Cr	Cu	Mn	Mo	Nb
0.053	0.004	0.0009	0.13	0.003	0.002	0.016	0.010	0.27	0.003	<0.001
Ni	P	Pb	S	Sb	Si	Sn	Ta	Ti	V	Zr
0.013	0.006	<0.001	0.008	0.001	0.023	0.001	0.006	0.002	0.002	0.001

TABLE 2 CHEMICAL COMPOSITION OF C1018 CARBON STEEL (WT.%) (FE IS IN BALANCE).

Al	As	B	C	Ca	Co	Cr	Cu	Mn	Mo	Nb
0.08	0.006	0.0009	0.20	0.001	0.011	0.061	0.028	0.90	0.018	0.014
Ni	P	Pb	S	Sb	Si	Sn	Ta	Ti	V	Zr
0.044	0.017	0.032	0.012	<0.001	0.044	0.011	0.023	0.005	0.004	0.007

TABLE 3 CHEMICAL COMPOSITION OF 5LX65 CARBON STEEL (WT.%) (FE IS IN BALANCE).

Al	As	B	C	Ca	Co	Cr	Cu	Mn	Mo	Nb
0.001	0.01	0.0007	0.16	0.001	0.019	0.017	0.062	0.80	0.016	0.010
Ni	P	Pb	S	Sb	Si	Sn	Ta	Ti	V	Zr
0.025	0.014	0.017	0.026	0.017	0.055	0.006	0.013	<0.001	0.002	0.006

TABLE 4 TEST MATRIX.

Liquid phase	D.I. water with 0, 0.1, and 1% NaCl
Gas phase	CO_2
Total pressure, bar	4.5, 7.9, 11.3, 14.8, 18.2
CO_2 partial pressure, bar	3.8, 7.8, 10.6, 14.8, 18.2
Temperature, °C	40, 90
Superficial gas velocity (V_{sg}), m/s	10
Superficial liquid velocity (V_{sl}), m/s	0.1
Flow regime	Stratified flow, annular flow
pH	as is, 5.2, and 6.2
Fe^{2+}, ppm	As measured. Most of the experiments start zero and end up with a few ppm Fe^{2+}. For Fe^{2+} concentration change during the tests, please refer to references 18 and 20 for the detail.

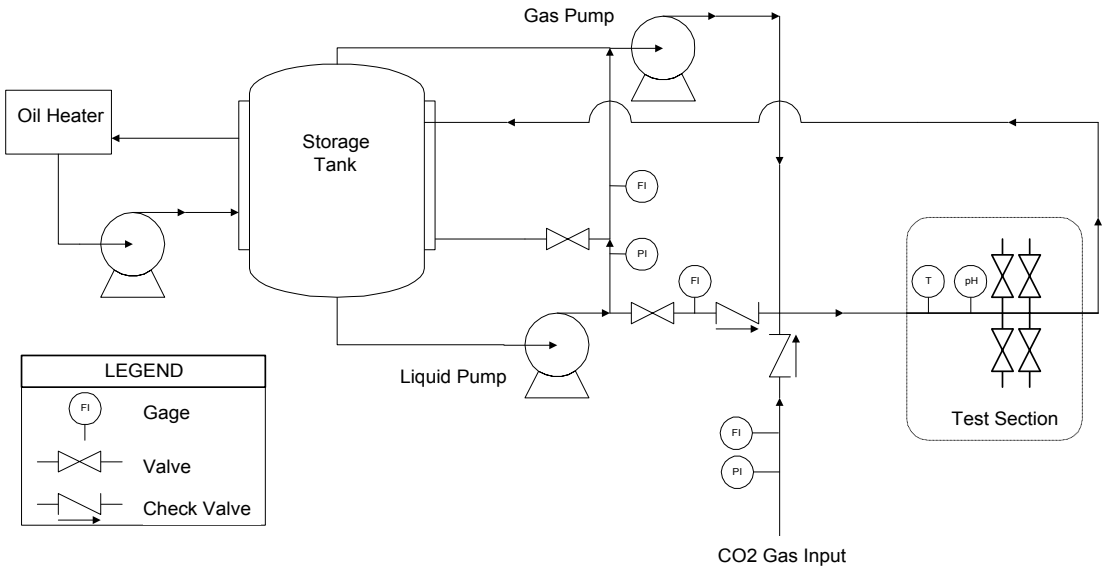

FIGURE 1. A schematic sketch of the test loop.

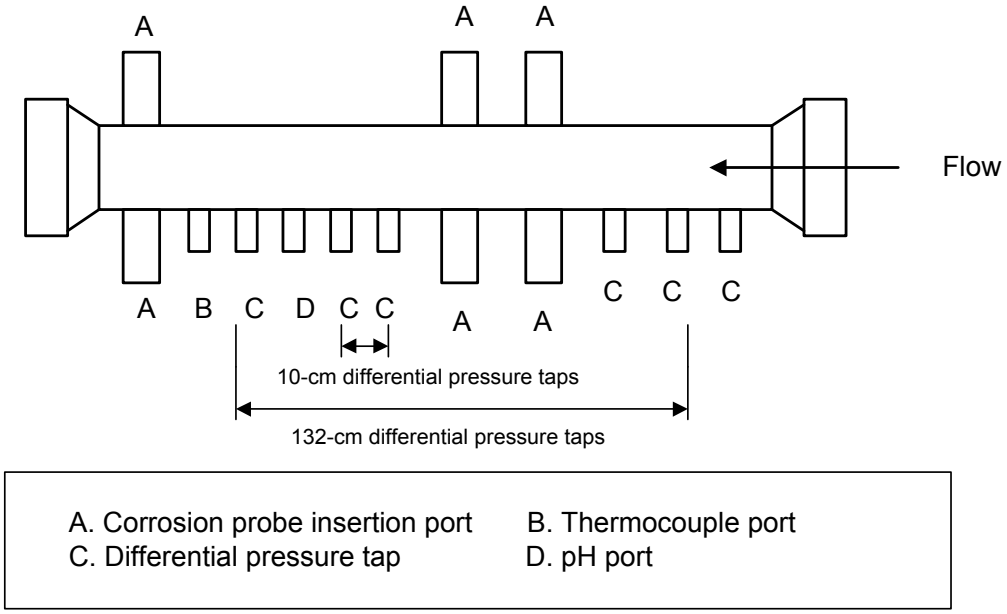

FIGURE 2. A schematic sketch of the test section.

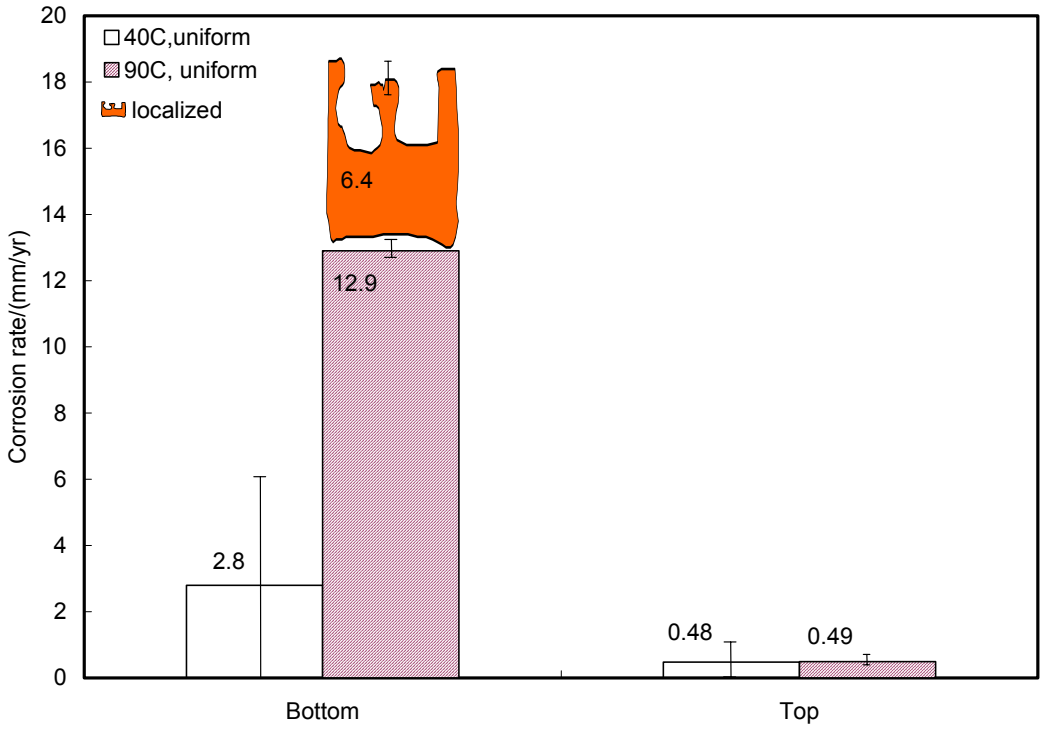

FIGURE 3. The effect of temperature on wet gas corrosion at V_{sl}=0.1 m/s, V_{sg}=10 m/s, and P_{total}=4.5 bar (P_{co2}=3.8 bar) with D.I. water only.

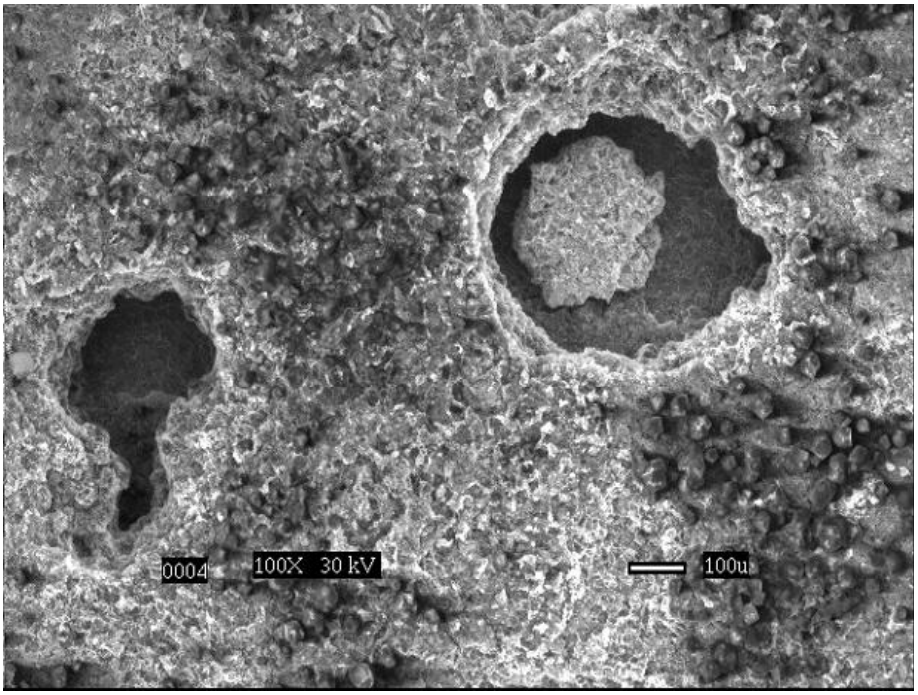

FIGURE 4. SEM surface morphology for 90°C bottom C1018 specimen at V_{sl}=0.1 m/s, V_{sg}=10 m/s, and P_{total}=4.5 bar (P_{co2}=3.8 bar) with D.I. water only.

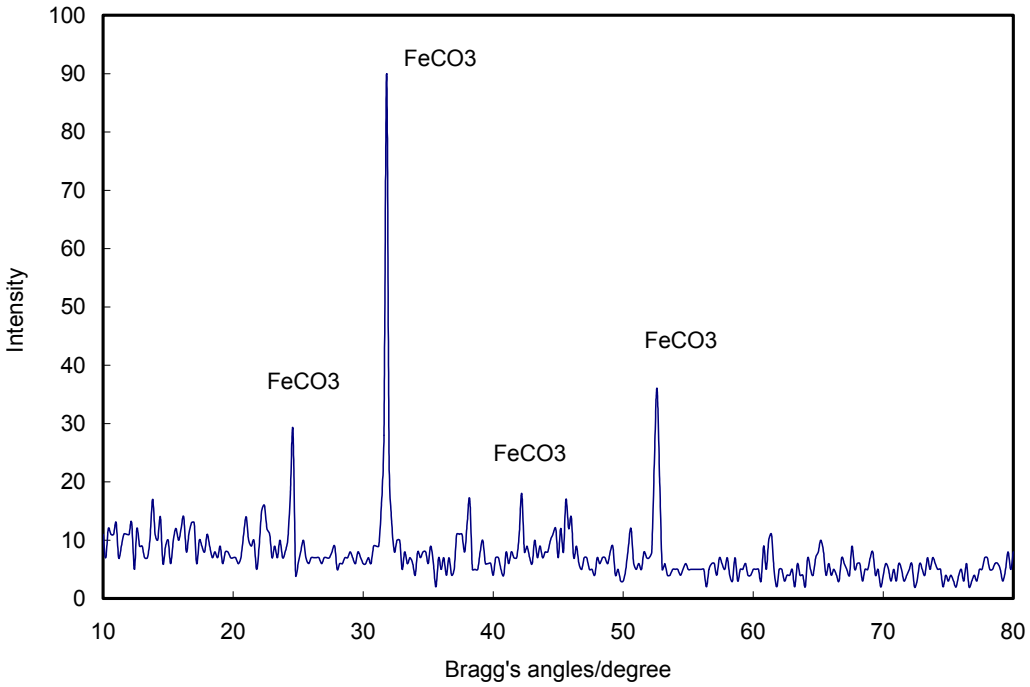

FIGURE 5. XRD spectrum for 90°C bottom C1018 specimen at V_{sl}=0.1 m/s, V_{sg}=10 m/s, and P_{total}=4.5 bar (P_{co2}=3.8 bar) with D.I. water only.

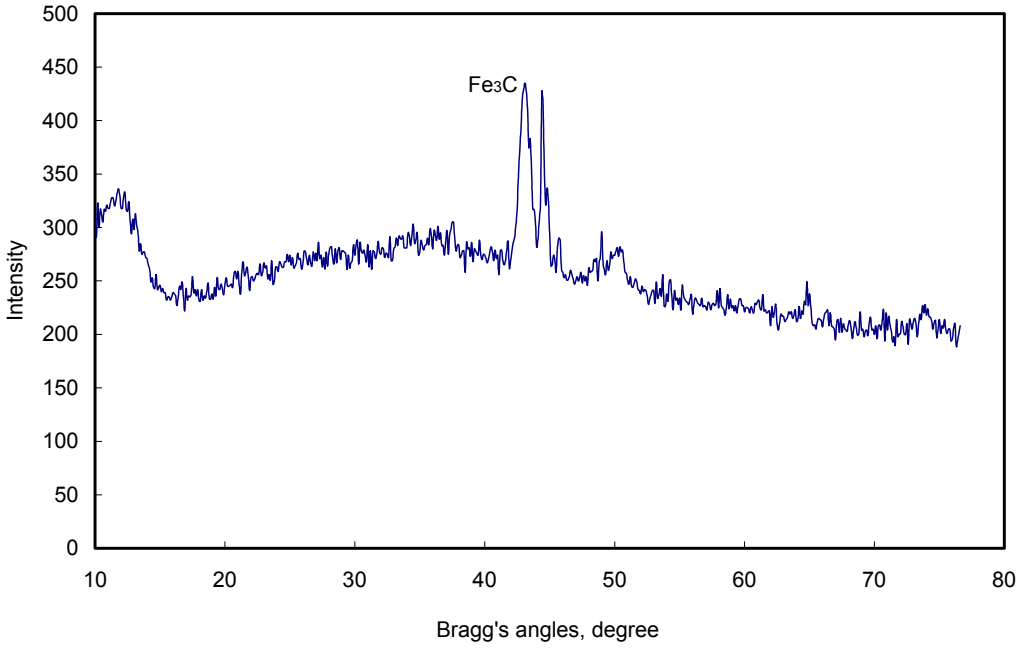

FIGURE 6. XRD spectrum for 40°C bottom C1018 specimen at V_{sl}=0.1 m/s, V_{sg}=10 m/s, and P_{total}=4.5 bar (P_{co2}=3.8 bar) with D.I. water only.

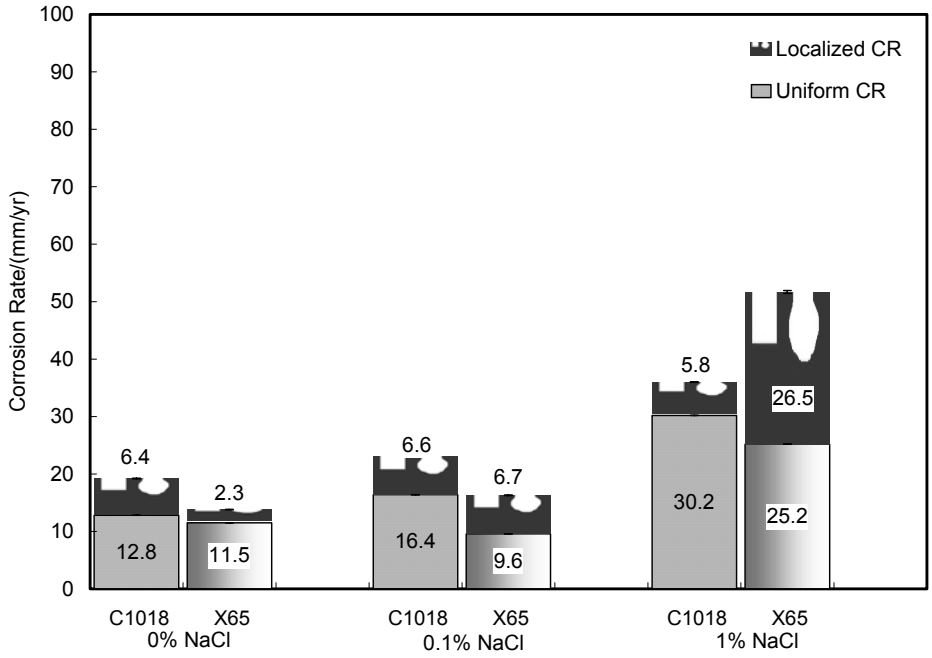

FIGURE 7. The effect of NaCl concentration on bottom corrosion for different materials from WL method at V_{sg}=10 m/s, V_{sl}=0.1 m/s, T=90°C, and P=4.5 bar (P_{co2}=3.8 bar).

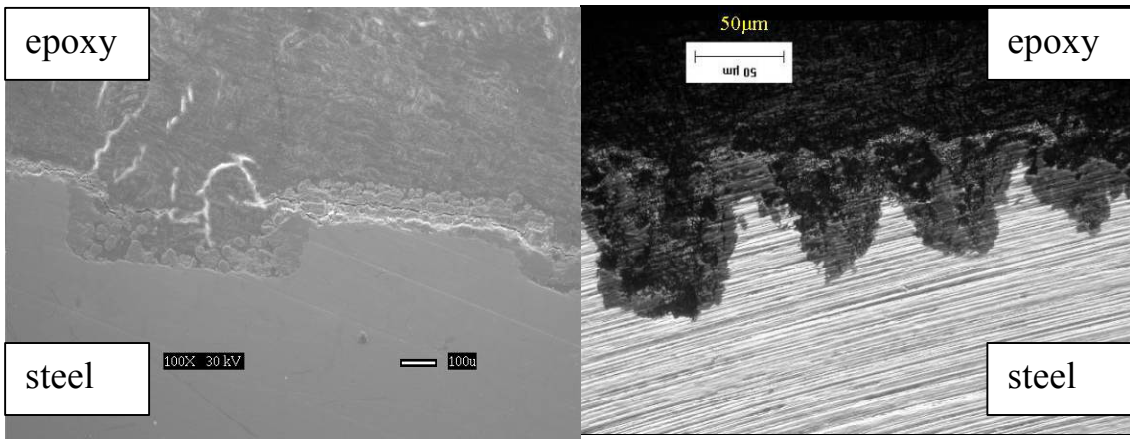

FIGURE 8. Cross sections for 0.0% Cl^- solutions at Vsg=10 m/s, Vsl=0.1 m/s, T=90°C, and P=4.5 bar (P_{co2}=3.8 bar). left: bottom C1018; right: bottom X-65.

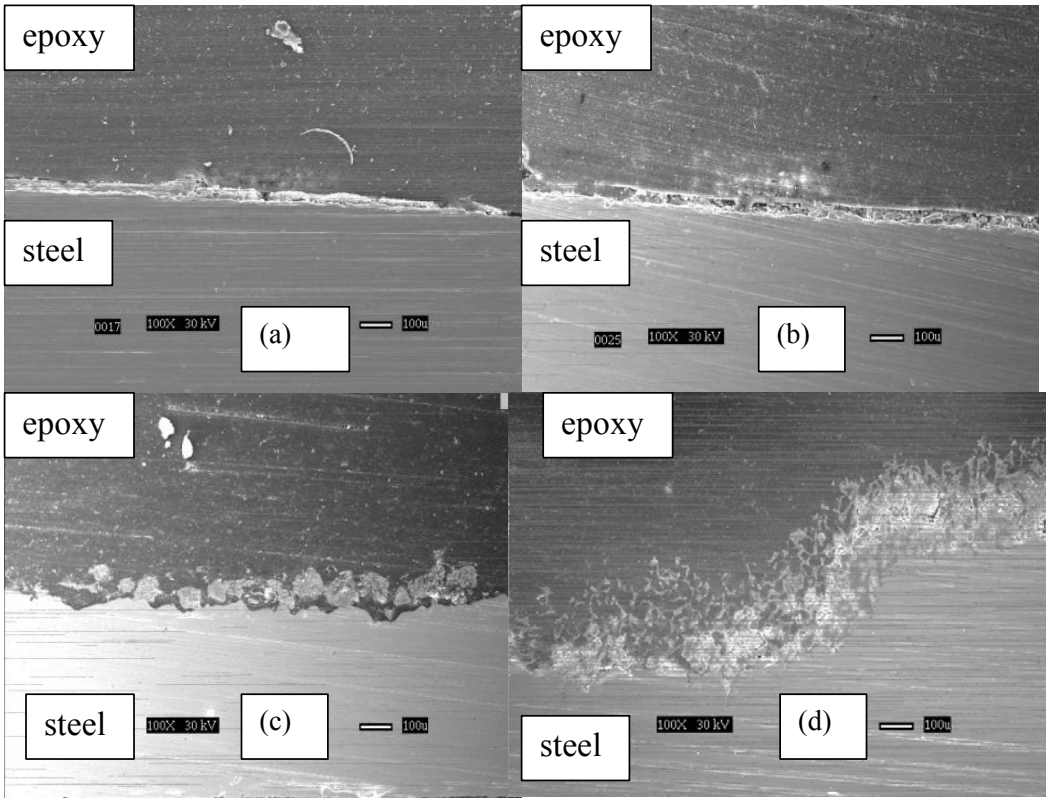

FIGURE 9. Cross sections for 1% NaCl solutions at V_{sg}=10 m/s, V_{sl}=0.1 m/s, T=90°C, and P=4.5 bar (P_{co2}=3.8 bar). (a) top C1018; (b) top X-65; (c) bottom ER C1010; (d) bottom X-65.

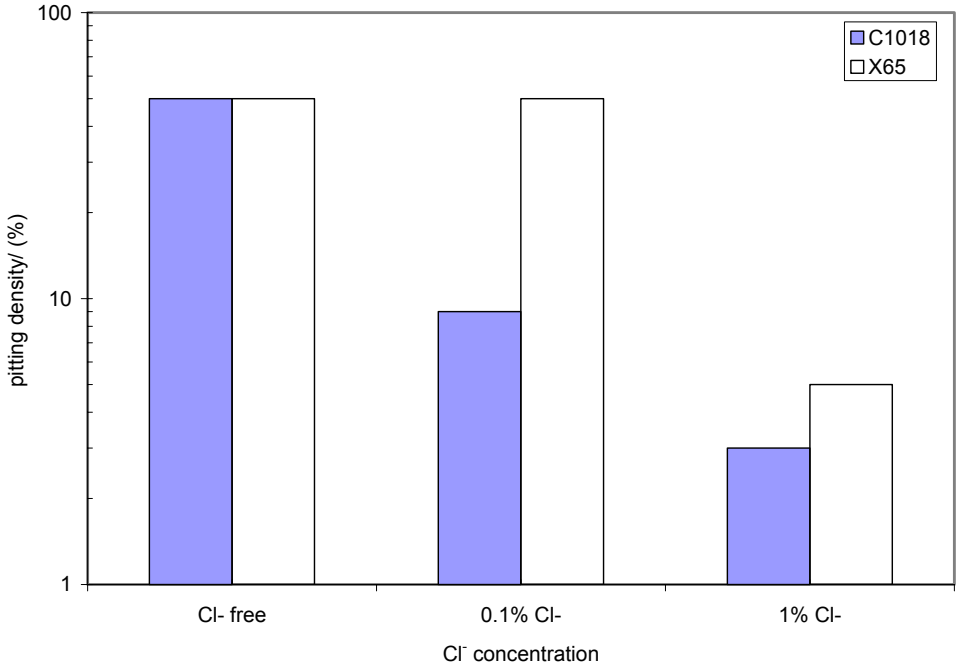

FIGURE 10. The effect of Cl^- concentration on localized corrosion at V_{sg}=10 m/s, V_{sl}=0.1 m/s, T=90°C, and P=4.5 bar (P_{co2}=3.8 bar).

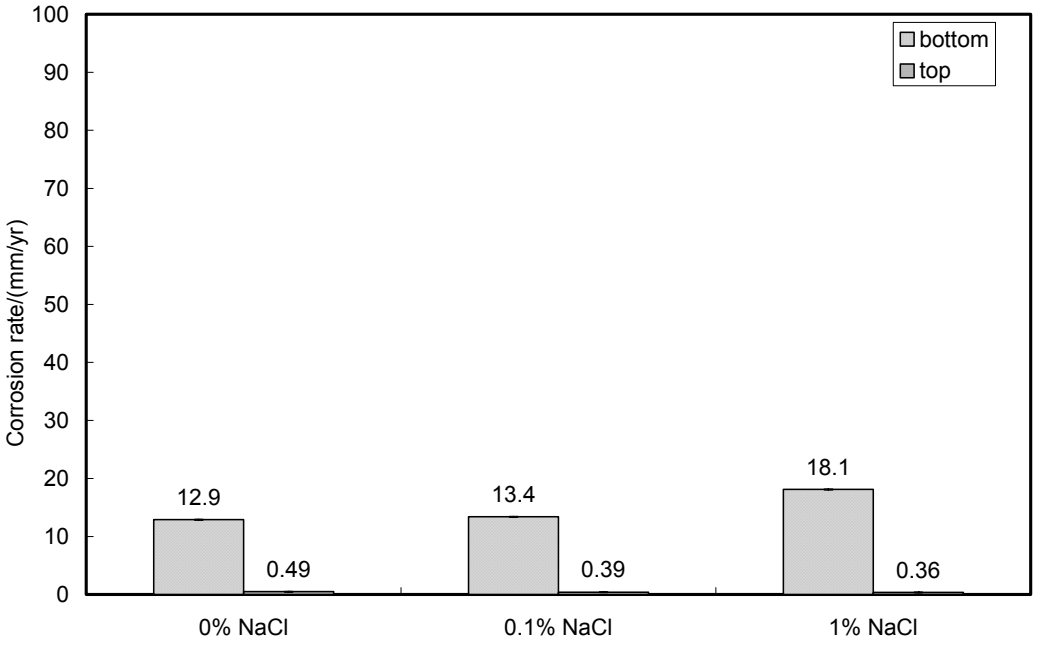

FIGURE 11. The effect of NaCl concentration on the average corrosion rate by ER measurements at Vsg=10 m/s, Vsl=0.1 m/s, T=90°C, and P=4.5 bar (P_{co2}=3.8 bar).

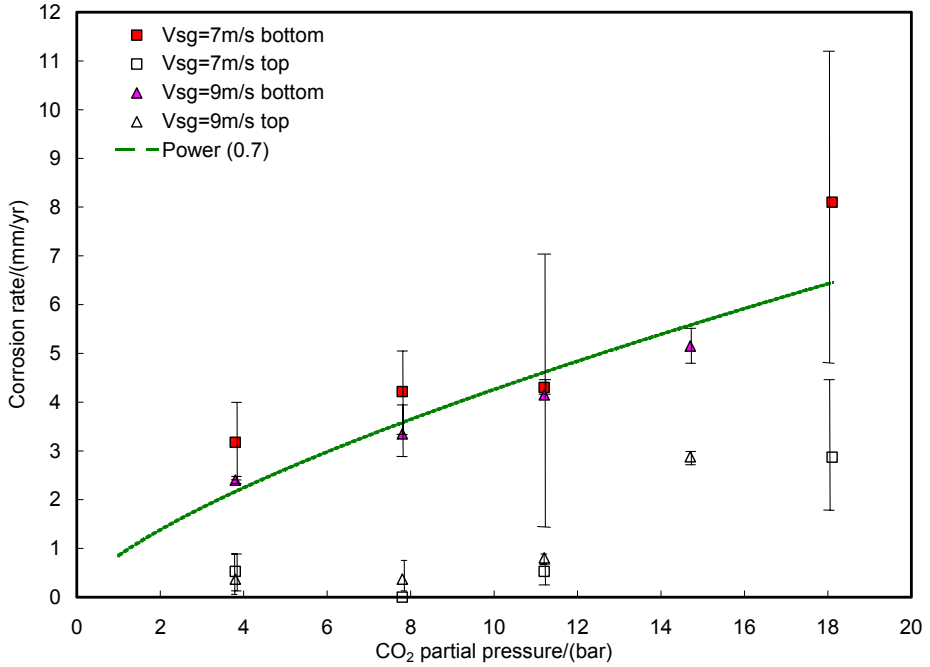

FIGURE 12. The effect of CO_2 partial pressure on both the top and the bottom corrosion rate at Vsl=0.1 m/s, T=40°C with D.I. water only.

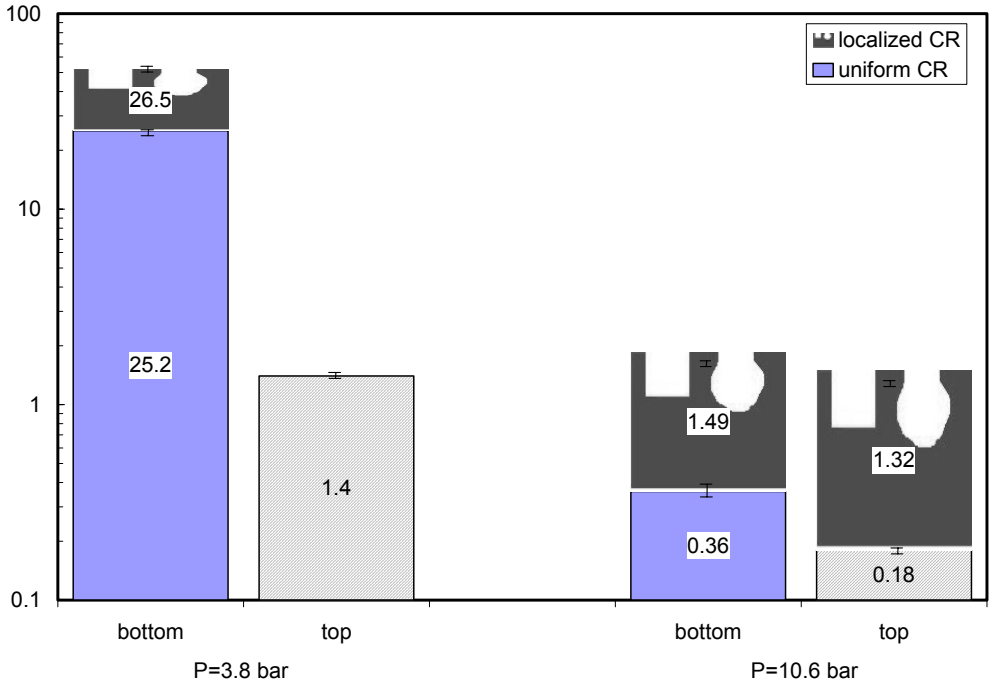

FIGURE 13. The effect of CO_2 partial pressure on the corrosion rate at low pH (≤5.2) from WL X65 steel at Vsl=0.1 m/s, Vsg=10 m/s, T=90°C with 1% NaCl solution.

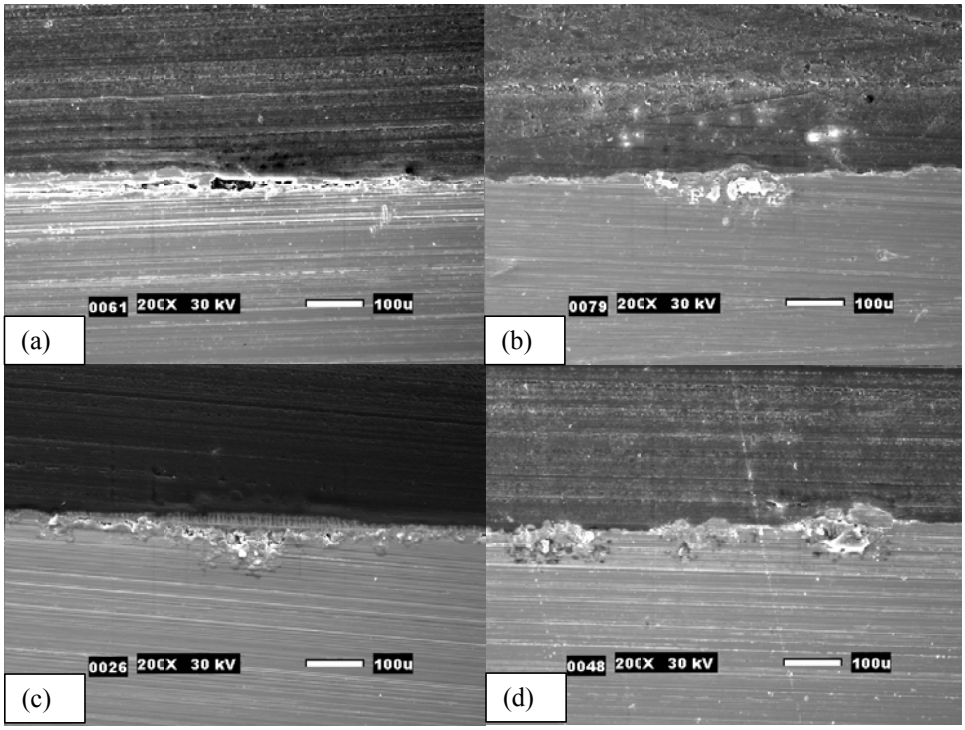

FIGURE 14. The change of corrosion rate with time for 1% NaCl at Vsg=10 m/s, Vsl=0.1 m/s, T=90°C, P=11.34 bar (P_{CO2}=10.64 bar), and pH=5.2.

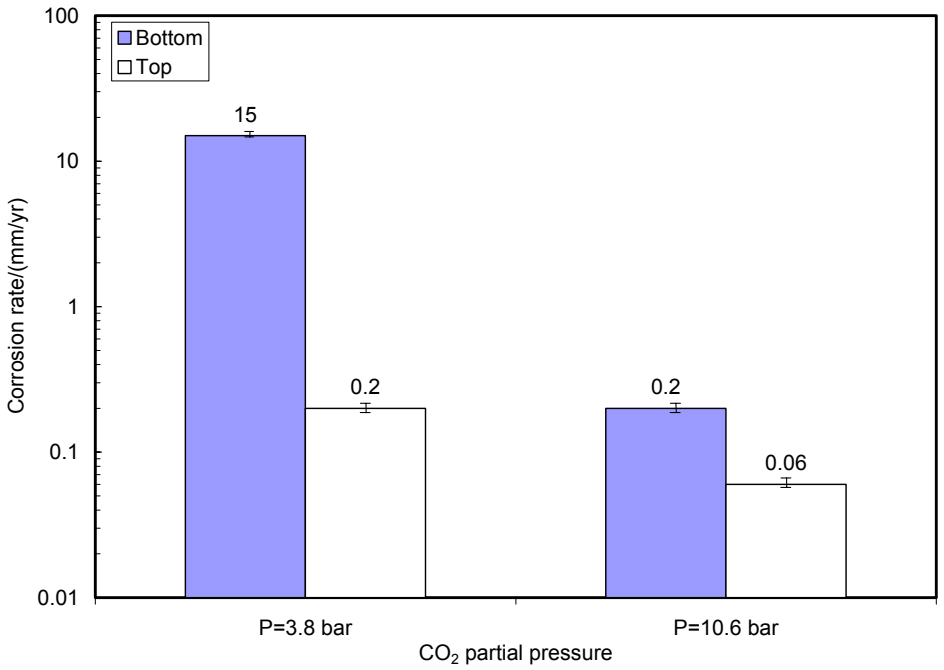

FIGURE 15. The effect of CO_2 partial pressure on stabilized corrosion rate at low pH (≤5.2) from ER technique at Vsl=0.1 m/s, Vsg=10 m/s, T=90°C with 1% NaCl solution.

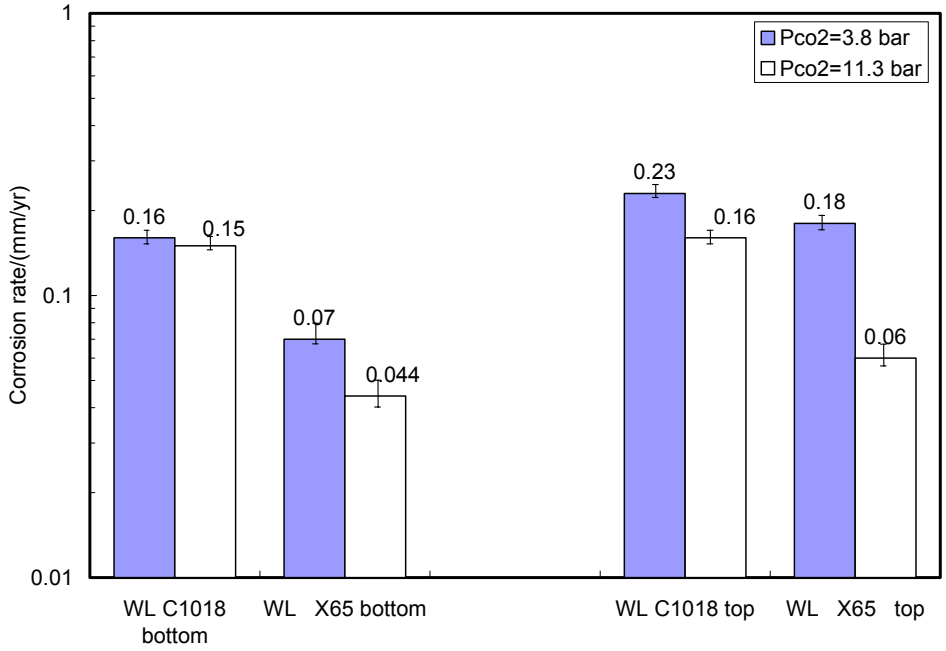

FIGURE 16. The effect of CO_2 partial pressure on the corrosion rate at high pH (6.2~6.3) from WL measurement techniques at Vsl=0.1 m/s, Vsg=10 m/s, T=90°C with 1% NaCl solution.

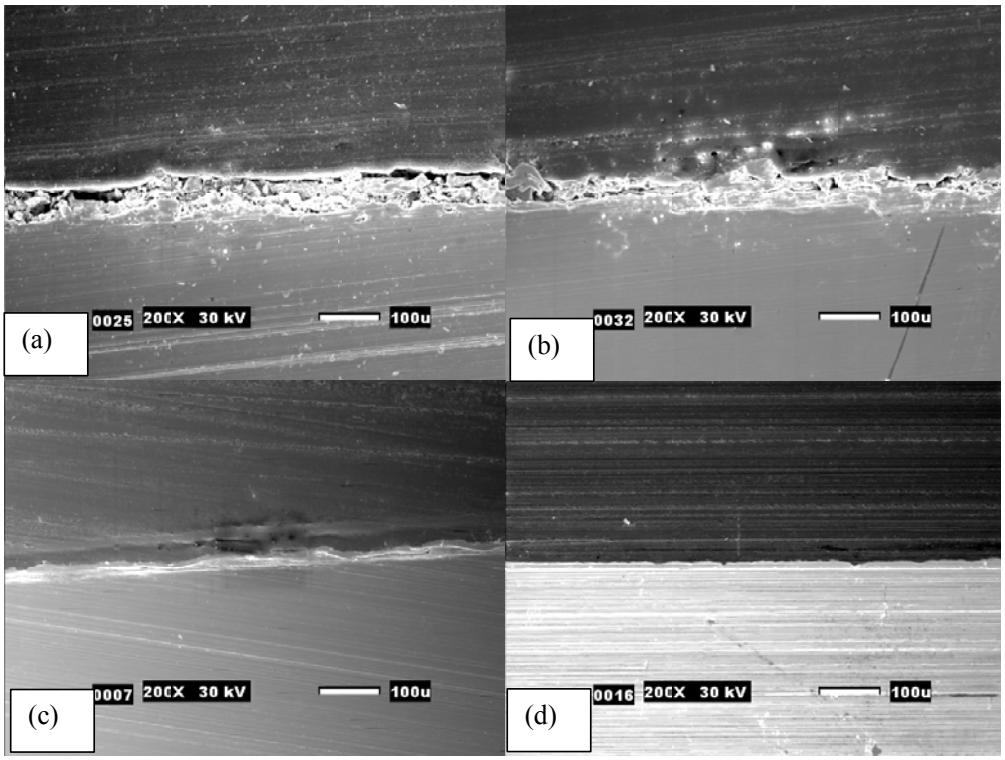

FIGURE 17. Cross sections for 1% NaCl at Vsg=10 m/s, Vsl=0.1 m/s, T=90 °C, P=11.34 bar (P_{CO2}=10.64 bar), and pH=6.2. (a) top C1018; (b) top X-65; (c) bottom C1018; (d) bottom X65.

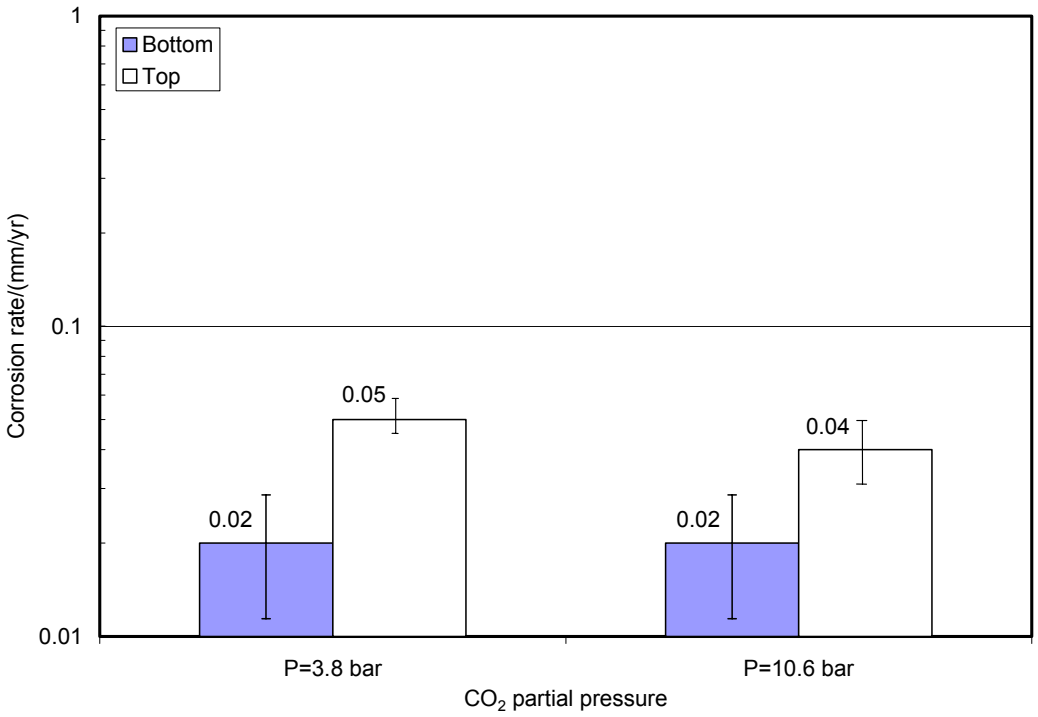

FIGURE 18. The effect of CO_2 partial pressure on stabilized corrosion rate at high pH (6.2~6.3) from ER technique at Vsl=0.1 m/s, Vsg=10 m/s, T=90°C with 1% NaCl solution.

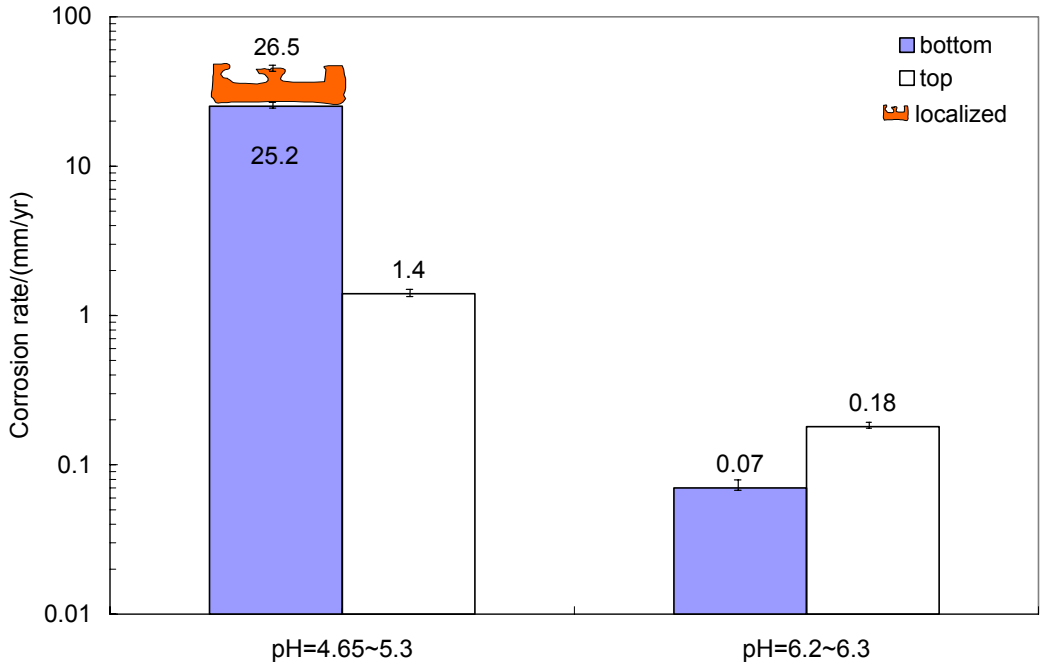

FIGURE 19. The effect of pH on the average and localized corrosion rate from WL X65 for 1% NaCl at Vsl = 0.1 m/s, Vsg = 10 m/s, T = 90°C, and P = 4.5 bar (P_{co2} = 3.8 bar).

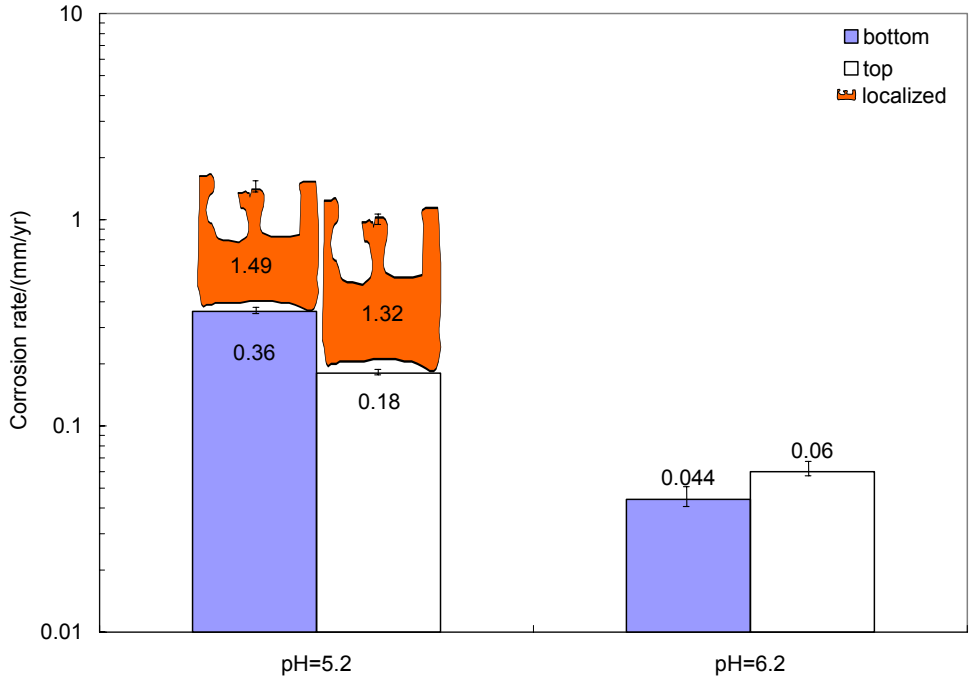

FIGURE 20. The effect of pH on average and localized corrosion rate from WL X65 for 1% NaCl at Vsl = 0.1 m/s, Vsg = 10 m/s, T = 90°C, and P = 11.3 bar (P_{co2} = 10.6 bar).

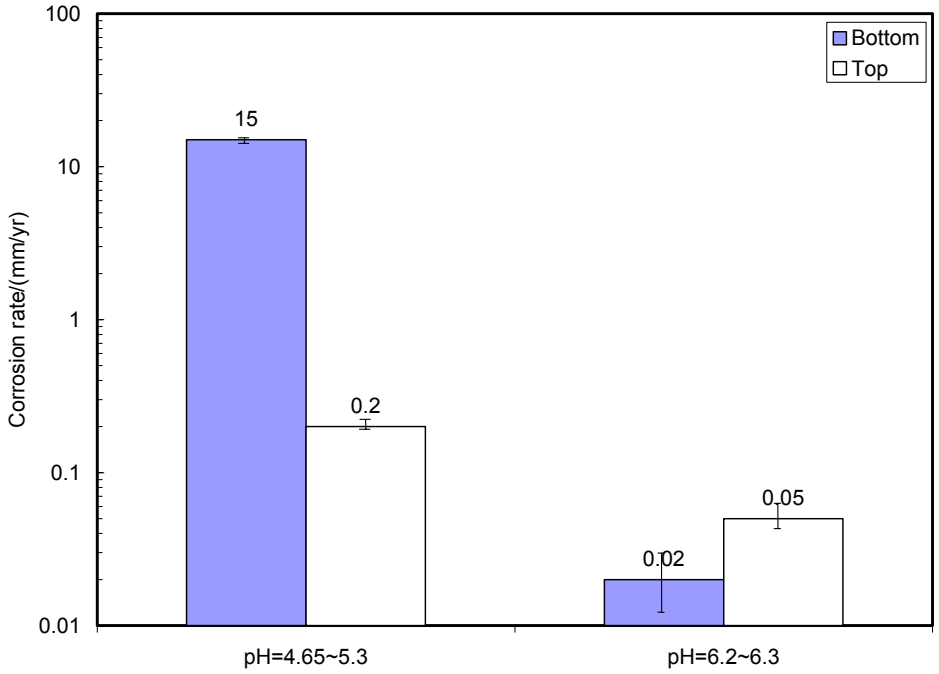

FIGURE 21. The effect of pH on the stabilized corrosion rate from ER method for 1% NaCl at Vsl=0.1 m/s, Vsg=10 m/s, T=90°C, and P=4.5 bar (P_{co2}=3.8 bar).

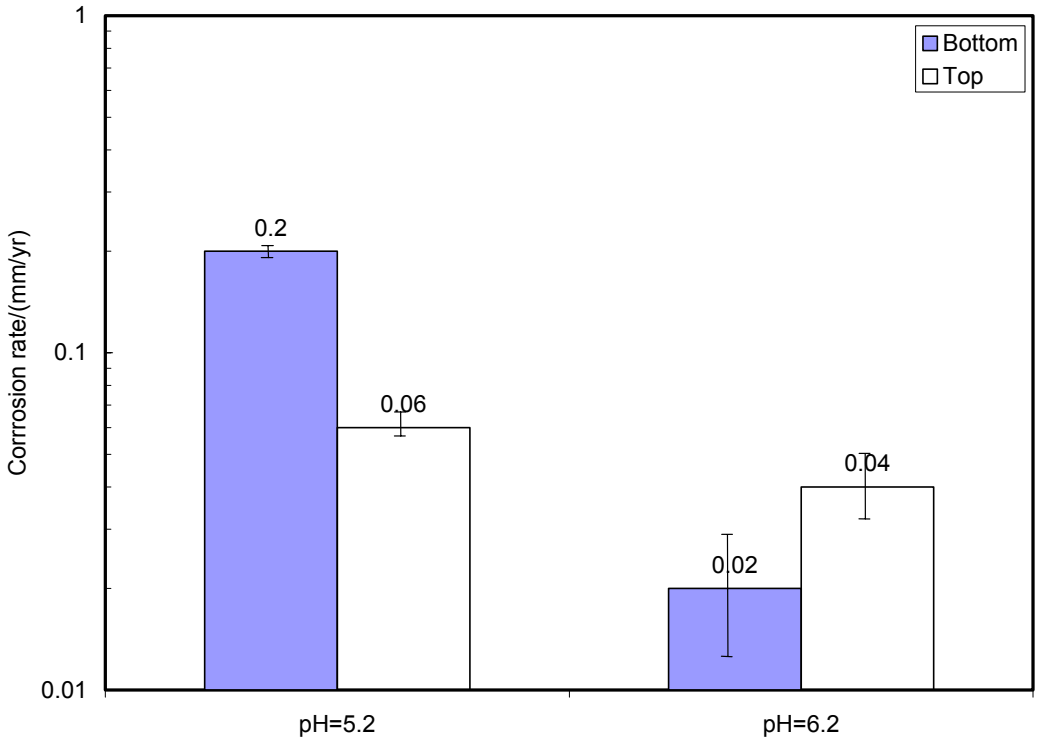

FIGURE 22. The effect of pH on stabilized corrosion rate from ER method for 1% NaCl at Vsl=0.1 m/s, Vsg=10 m/s, T=90°C, and P=11.3 bar (P_{co2}=10.6 bar).

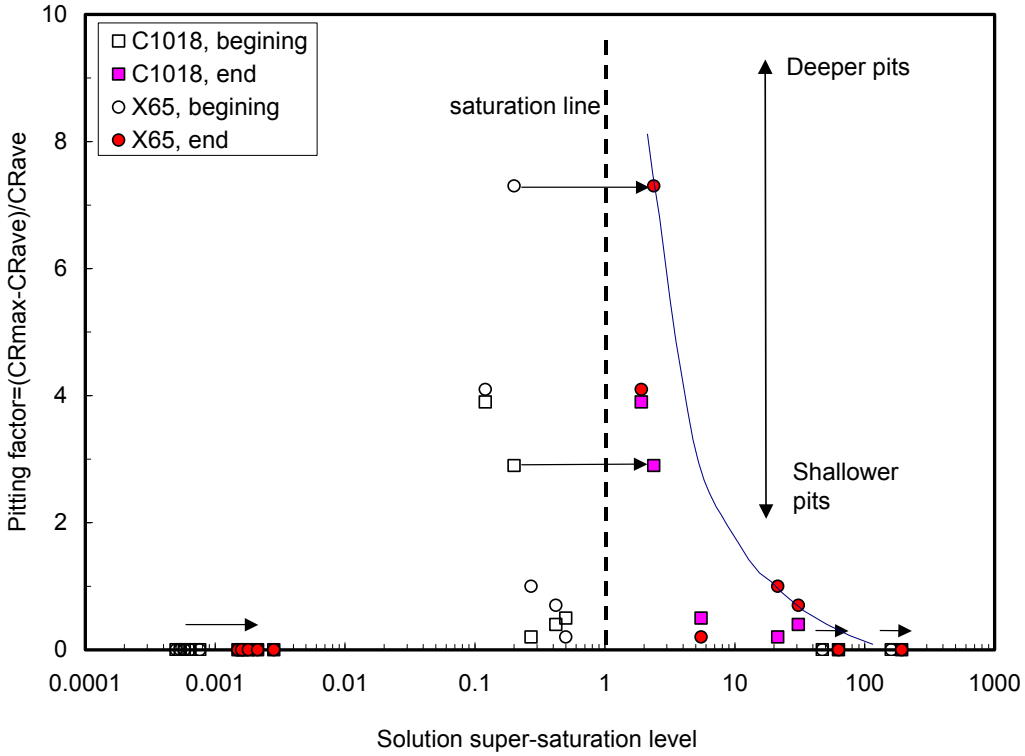

FIGURE 23. The relationship between the super saturation level and the pitting factor for all experiments.

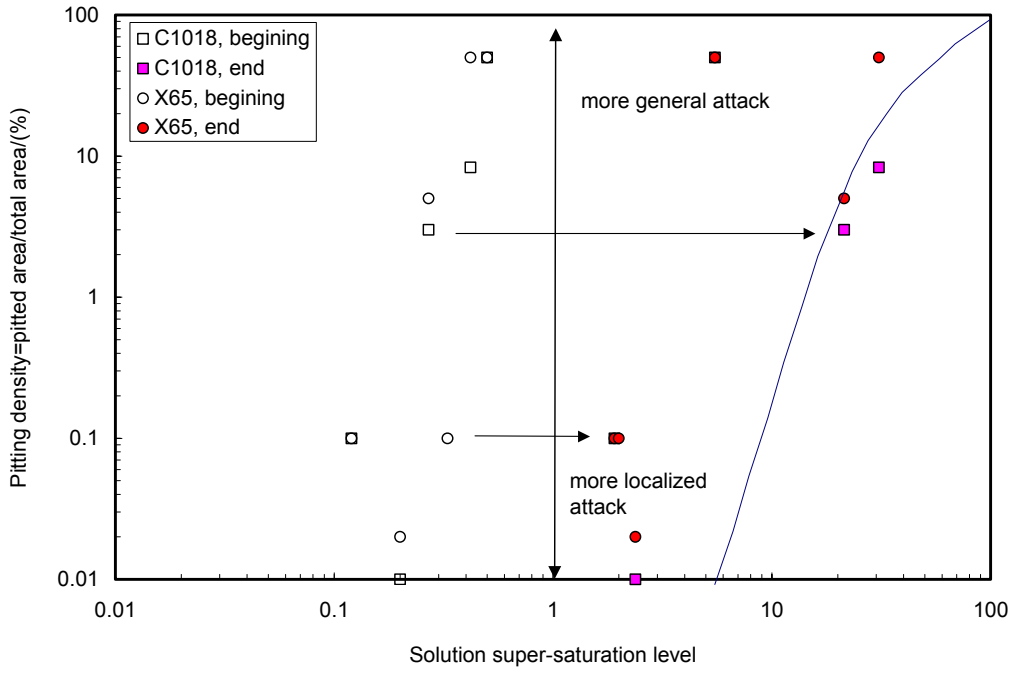

FIGURE 24. The relationship between the super saturation level and the pitting density for all experiments.

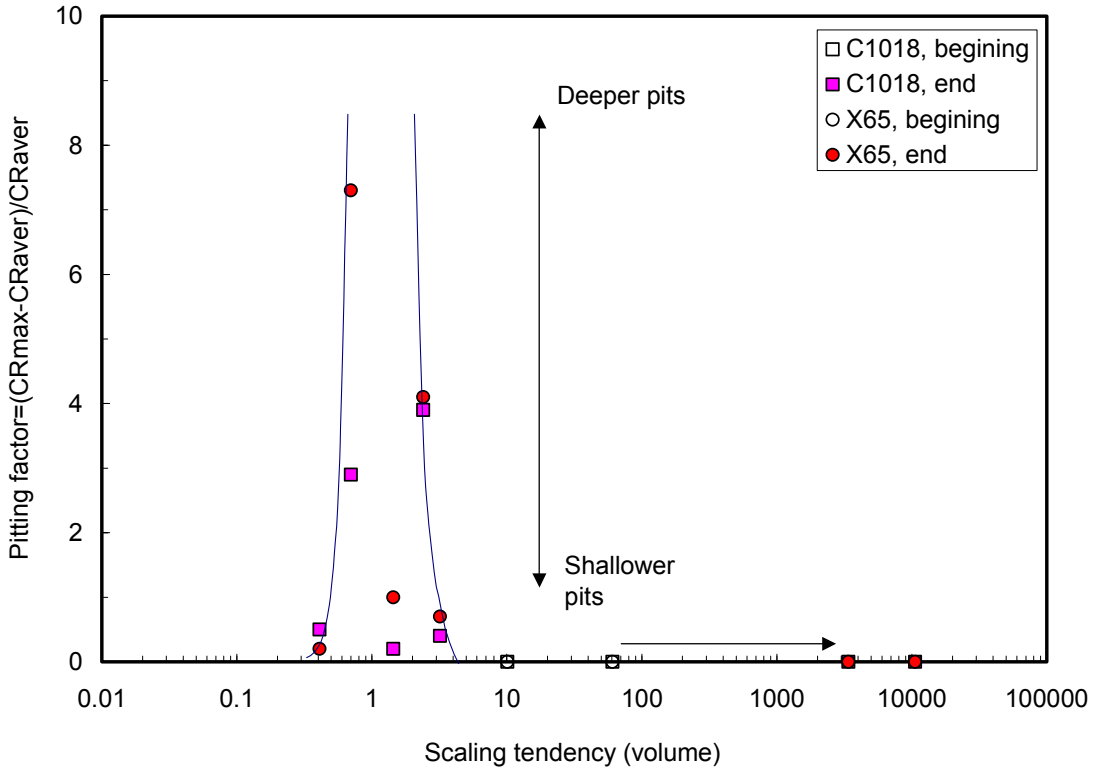

FIGURE 25. The relationship between the scaling tendency and pitting factor for all the experiments.